Journal Pre-proofs

Experimental sepsis-associated encephalopathy is accompanied by altered cerebral blood perfusion and water diffusion and related to changes in cyclooxygenase-2 expression and glial cell morphology but not to blood-brain barrier breakdown

Marion Griton, Ibtihel Dhaya, Renaud Nicolas, Gérard Raffard, Olivier Periot, Bassem Hiba, Jan Pieter Konsman

PII: S0889-1591(19)30877-3
DOI: https://doi.org/10.1016/j.bbi.2019.10.012
Reference: YBRBI 3883

To appear in: *Brain, Behavior, and Immunity*

Received Date: 13 August 2019
Revised Date: 2 October 2019
Accepted Date: 10 October 2019

Please cite this article as: Griton, M., Dhaya, I., Nicolas, R., Raffard, G., Periot, O., Hiba, B., Pieter Konsman, J., Experimental sepsis-associated encephalopathy is accompanied by altered cerebral blood perfusion and water diffusion and related to changes in cyclooxygenase-2 expression and glial cell morphology but not to blood-brain barrier breakdown, *Brain, Behavior, and Immunity* (2019), doi: https://doi.org/10.1016/j.bbi.2019.10.012

Experimental sepsis-associated encephalopathy is accompanied by altered cerebral blood perfusion and water diffusion and related to changes in cyclooxygenase-2 expression and glial cell morphology but not to blood-brain barrier breakdown

Marion Griton[a,b,c$] ,Ibtihel Dhaya[a,b,d$], Renaud Nicolas[a,b], Gérard Raffard[e,f], Olivier Periot[a,b,g], Bassem Hiba[a,b,h#] and Jan Pieter Konsman[a,b#*]

a INCIA, Institut de Neurosciences Cognitive et Intégrative d'Aquitaine, UMR 5287, Bordeaux, France

b Univ. Bordeaux, INCIA, UMR 5287, Bordeaux, France

c Service de Réanimation Anesthésie Neurochirurgicale, Centre Hospitalier Universitaire (CHU) de Bordeaux, Bordeaux, France

d Laboratoire de Neurophysiologie Fonctionnelle et Pathologies, UR/11ES09, Faculté des Sciences Mathématiques, Physiques et Naturelles, Université de Tunis El Manar, Tunis, Tunisia

e CNRS, Résonance Magnétique des Systèmes Biologiques, UMR 5536, Bordeaux, France

f Univ. Bordeaux, RMSB, UMR 5536, Bordeaux, France

g Service de Médecine Nucléaire, Centre Hospitalier Universitaire (CHU) de Bordeaux, Bordeaux, France

h CNRS UMR 5229, Centre de Neurosciences Cognitives Marc Jeannerod, Bron, France

Running title: CLP increases white matter axial diffusion

$ contributed equally to the present work; # co-senior authors

* Corresponding author:

Aquitaine Institute for Integrative and Cognitive Neuroscience (INCIA) UMR CNRS 5287,

University of Bordeaux, 146 rue Léo Saignat, 33076 Bordeaux, France

Phone / Fax: (33) 5 57 57 15 51 / (33) 5 56 90 14 21

Email: jan-pieter.konsman@u-bordeaux.fr

Abstract

Sepsis-associated encephalopathy (SAE) refers to brain dysfunction, including *delirium*, occurs during severe infection and is associated with development of post-traumatic stress disorder. SAE has been proposed to be related to reduced cerebral blood flow (CBF), blood-brain barrier breakdown (BBB), white matter edema and disruption and glia cell activation, but their exact relationships remain to be determined. In the present work, we set out to study CBF using Arterial Spin Labeling (ASL) and grey and white matter structure with T2- and diffusion magnetic resonance imaging (dMRI) in rats with cecal ligation and puncture (CLP)-induced encephalopathy. Using immunohistochemistry, the distribution of the vasoactive prostaglandin-synthesizing enzyme cyclooxygenase-2 (COX-2), perivascular immunoglobulins G (IgG), aquaporin-4 (AQP4) and the morphology of glial cell were subsequently assessed in brains of the same animals. CLP induced deficits in the righting reflex and resulted in higher T2-weighted contrast intensities in the cortex, striatum and at the base of the brain, decreased blood perfusion distribution to the cortex and increased water diffusion parallel to the fibers of the corpus callosum compared to sham surgery. In addition, CLP reduced staining for microglia- and astrocytic-specific proteins in the corpus callosum, decreased neuronal COX-2 and AQP4 expression in the cortex while inducing perivascular COX-2 expression, but did not induce widespread perivascular IgG diffusion. In conclusion, our findings indicate that experimental SAE can occur in the absence of BBB breakdown and is accompanied by increased water diffusion anisotropy and altered glia cell morphology in brain white matter.

Introduction

Sepsis-associated encephalopathy (SAE) refers to brain dysfunction ranging from mild *delirium* to deep coma that occurs in up to 70% of patients with severe systemic infection (Gofton and Young, 2012; Jones and Griffiths, 2013; Lamar et al., 2011; Young, 2013). In addition to acute mental dysregulation in the form of *delirium*, sepsis also has long-term detrimental effects on mental health. Indeed, clinical sepsis is associated with the development of post-traumatic stress disorders (PTSD) months later (Boer et al., 2008; Rosendahl et al., 2013; Schelling et al., 2001; Wintermann et al., 2015).

In spite of its impact on mental and cognitive health, the mechanisms underlying SAE are poorly understood (Chaudhry and Duggal, 2014). SAE, including *delirium*, has been proposed to be related to reduced cerebral blood flow (CBF) and oxygen extraction, blood-brain barrier breakdown (BBB), brain inflammation and edema (Chaudhry and Duggal, 2014; Papadopoulos et al., 2000; Tsuruta and Oda, 2016). Indeed, baseline CBF has been shown to be reduced during SAE (Bowton et al., 1989; Maekawa et al., 1991; Pfister et al., 2008; Pierrakos et al., 2013; Pierrakos et al., 2014; Smith et al., 1998; Yokota et al., 2003). Furthermore, systematic assessment of middle cerebral artery (MCA) blood velocity to variations in arterial blood pressure indicates that impaired cerebral autoregulation is associated with sepsis-associated *delirium* (Pfister et al., 2008; Schramm et al., 2012). Of note, some authors have also suggested that loss of cerebral autoregulation sepsis-associated contributes to edema during sepsis (Piazza et al., 2009).

Interestingly, and concomitantly with vasospasms in the MCA of patients with sepsis and brain dysfunction, T2- and diffusion-weighted Magnetic Resonance Imaging (MRI) have indicated white matter vasogenic edema (Bartynski et al., 2006; Sharshar et al., 2007). Moreover, in patients who died of sepsis, dilation of the perivascular space accompanied by dissociation of myelinated and white matter microglial activation have been observed

(Lemstra et al., 2007; Sharshar et al., 2007; Zrzavy et al., 2019). Finally, *delirium* has been found to be associated with disruption of white matter organization at hospital discharge and 3 months later, which, in turn, was associated with long-term cognitive impairment (Morandi et al., 2012). So among the proposed underlying mechanisms, clinical SAE has been shown to be associated with reduced CBF, signs of edema formation and white matter changes. However, the relationships between these phenomena and the occurrence and role of BBB breakdown as well as glial activation remain to be determined.

Experimental models allowing to systematically vary factors of interest have the potential to unravel the pathophysiological mechanisms underlying SAE. Intravenous administration of bacterial lipopolysaccharide (LPS) fragments in human volunteers is sufficient to reduce global CBF (Moller et al., 2002; Pollard et al., 1997). However, after systemic administration of LPS in animals, some studies have also observed rapidly decreased global or incoming CBF (Bryan and Emerson, 1977; Christenson et al., 1986; Ekstrom-Jodal et al., 1982; Tempel et al., 1986; Villega et al., 2017; Wyler et al., 1969; Wyler et al., 1972), whereas others studies have shown increased CBF in cortical MCA territories, but dose-dependent impaired autoregulation of CBF (Rosengarten et al., 2007; Rosengarten et al., 2008). And although peripheral LPS administration in rodents induces microglial activation in different brain structures (Hoogland et al., 2015), no study so far seems to have assessed white matter.

Cecal ligation and puncture (CLP) is a more clinically-relevant sepsis model than systemic LPS administration in that it involves live bacteria and mimics the different hemodynamic phases observed in clinical sepsis. Interestingly, during the first 24 h after CLP, CBF has been shown to be preserved (Hinkelbein et al., 2007) while increased T2-weighted contrast at the base of the brain suggested vasogenic edema and decreased apparent diffusion coefficient (ADC) indicated cytotoxic edema in the cortex and hippocampus (Bozza et al., 2010).

The aim of the present work was to establish temporal and spatial relationships between CNS

hemodynamic, metabolic and structural changes during experimental sepsis using imaging and histological approaches on brains of the same animals. We studied CBF and brain microstructure using Arterial Spin Labeling (ASL) and Diffusion-weighted Magnetic Resonance Imaging (dMRI), respectively, in animals with SAE 24h after CLP. In addition, we also detected the vasoactive prostaglandin-synthesizing enzyme cyclooxygenase-2 (COX-2), which is upregulated under inflammatory response, the presence of perivascular immunoglobulins G (IgG) as a measure of BBB integrity, and modifications of glia cell morphology in the brains of the same animals.

Materials and methods

Animals

Twenty-one male 3.5 month old Wistar rats (Charles River, l'Abresle, France) weighing 340.3 ± 3.6 g were used. Animals were treated according to European recommendations on animal research (European Council Directive of 24 November 1986 (86/609/EEC) and European Parliament and Council Directive of 22 September 2010 (2010/63/UE)), housed 2 per cage in a temperature-controlled room (22.0 ± 1.0°C) with lights on from 8 AM to 8 PM with free access to water and food. After arrival rats were left undisturbed for at least a week except for daily handling starting three days before surgery.

Surgery

On the day of surgery, animals were anesthetized with isoflurane (induction 3-5%; maintenance 1.5% in air). Once anesthetized, seventeen rats underwent polymicrobial intra-abdominal infection induced by CLP as previously described (Rittirsch et al., 2009; Wichterman et al., 1980). Briefly, after a 2-3-cm midline abdominal incision, the cecum was exposed in sterile saline on laboratory film (Parafilm, Neenah, WI, USA) and ligated with a 4-0 silk suture (Ethicon, Issy les Moulineaux, France) just below the ileocecal valve and subsequently punctured twice with a 22 G sterile needle. Next, a small drop of cecal contents was gently pushed out, before the cecum was gently placed back into the peritoneal cavity and the abdomen was sutured in two layers. At the end of the operation, animals received 5 ml of saline and analgesia (butrophanol, Torbugesic®; 2 mg/kg subcutaneously) and were placed in a clean individual cage. For the ten rats that were sham-operated rats, the same manipulations were performed except cecal ligation and puncture and saline injection. Thirty minutes after the end of surgery animals were awake and moving around.

Behavioral evaluation

To study non-specific sickness responses during sepsis, daily food and water intake and body weight were measured at several time points prior and posterior to surgery.

Delirium involves, according to the *Diagnostic and Statistical Manual of Mental Disorders*, disturbances of consciousness or awareness and in attention (Meagher et al., 2014), and is therefore hard to assess in animals. However, SAE is routinely monitored through assessment of reflexes, for example as part of the Glasgow coma scale (Ebersoldt et al., 2007), and can thus be easily and robustly implemented in animals. Following Kadoi & Goto (2004), sham and CLP -operated rats were tested at different time points before and after surgery for two simple non-postural (pinna and corneal reflexes) and one complex postural somatomotor reflex (righting reflex).

The pinna reflex was assessed by lightly touching the auditory meatus with a cotton stick tip and recording the occurrence and rapidity of ear retraction or head shake. The corneal reflex was tested by gently touching the cornea with a cotton stick tip and scoring the occurrence and rapidity of eye blinks. The righting reflex consisted of picking up the animal behind the forepaws and holding its trunk horizontally back upwards before putting the animal's back down and evaluating the time required to turn over to an upright position.

Magnetic Resonance Imaging (MRI) acquisition and image processing

Twenty-four hours after surgery, animals were anesthetized again with isoflurane (induction 3-5%, maintenance 1.5%) and introduced into a 7T horizontal-bore scanner (Advance III console, Bruker, Ettlingen, Germany) equipped with a magnetic field gradient system providing a maximum magnetic field gradient amplitude of 650 mT/m. A quadrature coil was used for radio-frequency emission and a 4-element phased-array surface coil for signal reception. Intracolonic temperature was constantly monitored and the animal was heated

when colonic temperature dropped below 35.5°C by warm water circulating in the bed used to position the rat inside MRI scanner. Respiration was assessed with a ventral pressure sensor and heart rate recorded using an MRI compatible electrode. After careful second-order shimming, T1-weighted MRI, T2-weighted MRI, Arterial Spin Labeling (ASL) and diffusion-weighted MRI (dMRI) images were acquired (see supplementary Materials and Methods for details of MRI acquisition sequences).

Analysis of T2-weighted images was performed using mipav (https://mipav.cit.nih.gov). In this study, relative T2-weighted intensities were compared to determine the presence rather than the quantity of edematic fluid (Abdel-Aty et al., 2005). Volumes Of Interest (VOIs) were defined in the brain and in the skull muscles and expressed as ratios. The VOI at the base of the brain was made up of 3 parts (right, left and center) to avoid blood vessels. The corresponding VOIs were summed together to cover the base of the rat brain (in bregma ~ -0.46mm). The other VOIs were cortex, striatum (right and left) and corpus callosum. Maximum and average intensities obtained in brain VOIs were then divided by those obtained in the skull muscle.

ASL data processing was performed using ParaVision software (Bruker, Ettlingen, Germany) unless otherwise indicated. Two (selective and global) T1 maps were computed using slice-selective and global FAIR data sets. Relative cerebral blood flow (rCBF) map was then computed pixel by pixel according to Kober et al. (2004). Blood T1 measured on rat blood at 7 T was set at 2070 ms (Dobre et al., 2007; Esparza-Coss et al., 2010). To analyze perfusion data, Regions Of Interest (ROIs) corresponding to the global brain, brain hemispheres, grey matter of the cortex and striatum as well as to the white matter of the corpus callosum and external capsule were traced manually on each individual's selective inversion 1100ms FAIR image using a rat brain atlas (Swanson, 1998) for guidance. These ROIs were then copied onto perfusion maps images (Fig. 1).

A quality control was first performed on raw dMRI data and diffusion tensor imaging (DTI) maps. The *3dSkullStrip* command included in Analysis of Functional NeuroImages software (AFNI) (https://afni.nimh.nih.gov) was used for image processing 1) to extract the brain from surrounding tissues and 2) to create a mask. The twenty-one DW images and the B0 images were corrected for eddy currents using *eddy* and fitted to the DTI model with *dtifit* (both part of the FMRIB's Software Library (FSL) (http://www.fmrib.ox.ac.uk/fsl)).

The following diffusion-tensor maps were computed: 1) Eigenvalues (λ1, λ2 and λ3) corresponding to water molecule diffusivities along the principal axes of the diffusion tensor, 2) Axial Diffusivity (AD=λ1) representing water diffusivity along the length of the white matter fibers, 3) Radial Diffusivity (RD=(λ2+λ3)/2)) representing water diffusivity perpendicular to the white matter fibers. 4) Mean Diffusivity (MD=(λ1+λ2+λ3)/3) of water molecules, 5) Fractional Anisotropy (FA calculated following Alexander (2000)) indicating the degree of anisotropy of water diffusivity and 6) residuals maps as a quality assessment tool for DTI regression accuracy showing artefacts that are not always visible on above maps. Additional maps were then calculated to describe the shape of diffusion including 7) Coefficient of sphericity (Cs) corresponding to the roundness of tensor ellipsoid, 8) Coefficient of planar anisotropy (Cp) measuring planarity, and 9) Coefficient of linear anisotropy (Cl) that assesses the tendency of the tensor ellipsoid to have a cigar shape (Alexander et al., 2000).

ROIs were positioned manually on the white matter of the corpus callosum and external capsule and the grey matter of the cortex and striatum at two different rostrocaudal levels: 1) bregma -0.51mm (Swanson, 1998) and 2) bregma -1.08mm (Swanson, 1998) because the cytoarchitecture of these structures is known to vary along the rostrocaudal axis (Barazany et al., 2009). On Color-coded FA maps showing white matter in different colors according to fiber orientations, additional ROIs were placed on the cortex and on the external capsule,

after which the part of the external capsule where axons run horizontally and the part where axons are oriented vertically were analyzed.

To explore diffusion data in a non-hypothesis driven manner, a whole brain voxelwise statistical method adapted to the rat brain was performed using Tract-Based Spatial Statistics (TBSS) which is part of FSL (Smith et al., 2006). FA maps from each rat were co-registered to the DTI Rat Atlas for Postnatal Day 72 (DTI-RAPnD72) template (https://www.nitrc.org/projects/dti_rat_atlas/) using *fnirt* a nonlinear registration command adapted to take into account rat brain. After image registration, FA maps were averaged to produce a group mean FA image. A skeletonization algorithm was applied to the group mean FA image to define a group template of the lines of maximum FA, thought to correspond to centers of white matter tracts. FA values for each individual subject were then projected onto the group template skeleton by searching along perpendiculars from the skeleton to find local maxima. Non-FA maps (AD, RD, and MD) were skeletonized according to non-linear warps of the FA registrations described above.

Tissue processing and immunohistochemistry

At the end of MRI, rats were deeply anaesthetized by intraperitoneal injection of 60mg/kg of sodium pentobarbital. Bodies were rinsed from blood by intracardiac perfusion with 0.1 M phosphate-buffered saline (PBS; pH 7.4) and subsequently fixed by 300 ml of 4% paraformaldehyde in 0.1 M PBS. Brains were removed from the skull, post-fixed for 4 h in the same fixative, and then cryoprotected in 30% sucrose in 0.1 M phosphate buffer. Thirty-micrometer thick sections were cut on a cryostat (CM3050 S, Leica Microsystems, Nussloch, Germany) from the rostral limit of the optic chiasm to the caudal end of the central amygdala (Swanson, 1998) and collected in cold cryoprotectant solution (0.05 M PBS, 20 % glycerol, 30% ethylene glycol) and stored at -20°C until processing.

Immunohistochemistry was performed as previously described (Konsman and Blomqvist, 2005; Konsman et al., 2008; Konsman et al., 2004). Briefly, free-floating sections were washed four times in 0.1 M PBS (pH 7.4). Non-specific binding sites were blocked by a 45-minute incubation of sections in PBS containing 0.3% Triton X-100 and 2.0% normal serum or 1.0% BSA. The first antibody was then diluted (indicated below for every antiserum used) in the same buffer and added to the sections overnight at room temperature.

Commercially available antisera raised against COX-2 (goat anti-COX-2; M-19 sc-1747, lot# F2512, Santa Cruz Biotechnology, Heidelberg, Germany) diluted 1:750, the microglia-macrophage specific ionized calcium-binding adaptor molecule (Iba-1; rabbit anti-Iba-1; 019-19741, Wako Chemicals GmbH, Neuss, Germany) diluted 1:1000 and rat immunoglobulin G (IgG; biotinylated goat anti IgG, BA-9401, Vector Laboratories, Burlingame, CA, USA) diluted 1:2000, the astrocytic aquaporin-4 water channel (rabbit anti-AQP4, cat # AB2218, lot # 2506432, Millipore, Fontenay sous Bois, France) diluted 1:2000, the intermediate filament Glial fibrillary acidic protein GFAP (mouse anti-GFAP mAb, clone GA5, MAB360, Merck Millipore, Fontenay sous Bois, France) diluted 1:500, the myelin-associated enzyme 2',3'-Cyclic-nucleotide 3'-phosphodiesterase also known as CNPase (mouse anti-CNPase, Abcam, Paris, France) diluted 1:8000 were used.

After four rinses in PBS, sections were treated for 30 minutes with 0.3% (v/v) hydrogen peroxide to block endogenous peroxidases followed by four rinses in PBS. With the exception of those sections exposed to biotinylated rat IgG, sections were then incubated for 2h with biotinylated antisera raised against IgGs of the species of the first antibody (Vector Laboratories, Burlingame, CA, USA) diluted 1:500 in PBS, 0.3% Triton X-100, 1% BSA or normal serum. After four washes in PBS, sections were incubated for 2 h with avidin and biotinylated peroxidase complex (Vector Laboratories, Burlingame, CA, USA) diluted in PBS to 1:750 in IgG immunostaining and 1:500 in others. Finally, sections were transferred

to a sodium acetate buffer (0.1 M; pH 6.0) and stained using diaminobenzidine as a chromogen in the presence of Ni-ions, thus yielding a dark grey to black precipitate.

Microscopy and image analysis

Staining reactions were stopped by rinses in sodium acetate and PBS, after which sections were mounted on slides in 0.5% gelatin in distilled water containing chromo-potassium sulphate, dehydrated in alcohol, defatted in xylene and coverslipped with Eukitt (O.Kindler GmbH & CO, Freiburg, Brisgau, Germany). Stained sections were examined with a light-microscope (Leica DM5500B, Leica Microsystems, Nanterre, France) and images were captured by a high-resolution digital camera system (Leica DFC425C, Leica Microsystems, Nanterre, France) and stored onto a personal computer. In every brain section between bregma +4,85 and -2,85 mm the occurrence and extent (scored as restricted (1), intermediate (2) or extensive (3)) of perivascular IgG diffusion in a given structure was noted. As each region or structure considered covered at least two, but a varying number (depending on the length of the structure), of brain sections (with two consecutive sections being separated by 240 μm), the number of occurrences of perivascular IgG diffusion for a structure were then divided by the number of brain sections in which the structure was present. Similarly, the cumulative score of the extent of IgG diffusion for a given brain region or structure was also divided by the number of sections that contained the region or structure in question.

The counts and relative surfaces of AQP4, CNPase, COX-2, GFAP and Iba-1-immunoreactive elements were quantified after application of fixed particle size and intensity criteria on 8-bit images with Image J (http://imagej.nih.gov/ij/). Iba-1- and GFAP-immunostaining was also quantified using the Image J plugin Fraclac (http://rsb.info.nih.gov/ij/plugins/fraclac/fraclac.html). Briefly, on binary images of brain sections between bregma -0.11 and -1.33 mm, Iba-1-positive cells (size between 300-6000

pixels) and GFAP-immunoreactive cells (size between 300-8000 pixels) were enclosed by a Hull convex (a boundary enclosing the foreground pixels of an image using straight line segments to each outermost point) and bounding circle after which the surface, perimeter, diameter and circularity (defined as $4*\pi*\text{Area} / \text{Perimeter}^2$) were determined in addition to the width and height of the cells. In addition, Iba-1 cell size and activation was also evaluated with Image J based on staining intensity as described by Hovens et al (2014). Briefly, a minimum size filter was applied on cell body size (>150 pixels) before cell and cell body size were distinguished based on an intensity criterion. Finally, three different categories of sizes of GFAP-positive elements (GFAP: <300 pixels considered as astrocytic fragments; 300<pixels<8000 considered as astrocytes; pixels>8000 considered as astrocytes in contact) were quantified in terms of number and relative surface after application of a fixed intensity threshold.

Image editing software (Adobe Photoshop, Adobe Systems, San Jose, CA, USA) was used only to adjust contrast and brightness for photomicrographs composing illustrating figures.

Data representation and analysis

Food intake and water intake were expressed relative to 100g of body weight and 100g of food intake respectively. Maximum intensity obtained from T2-weighted images analysis was expressed relative to skull muscle. To assess blood redistribution between brain structures, ASL values in cerebral structures were also expressed relative to perfusion of brain hemispheres or to that of the global brain parenchyma in the case of the corpus callosum that is situated between the two hemispheres. All data, except TBSS data, were expressed as means ± standard error of the mean (SEM) and analyzed by a one-way ANOVA with surgery as a between factor. When data were not normally distributed, a log10 or square root transformation was performed, and if still not normally distributed then the non-parametric

Mann-Whitney U test was used. Pearson linear correlation coefficients were calculated between MRI (T2, ASL and DTI) parameters and immunohistochemical (AQP4-, COX-2-, GFAP- and Iba-1-immunoreactivity) data. In all cases, a level of $p<0.05$ was considered as statistically significant.

For statistical analysis of TBSS data, a nonparametric voxel-wise statistical procedure was carried out using *randomise,* a permutation testing algorithm, with 500 and 5000 permutations. Threshold-free cluster enhancement (TFCE) method (Smith and Nichols, 2009) was used to define clusters with significant differences at $p < 0.05$ fully corrected for multiple comparisons across space. Contrasts were performed for sham-operated vs. CLP animals. TBSS results were displayed on top of the group mean_FA map, the DTI-RAPnD72_template and the DTI-RAPnD72_labels.

Results

CLP reduced food intake and induced encephalopathy

Within the 23h following the end of surgery, no mortality was observed in the sham-operated group (One animal did die however at the induction of anesthesia for imaging) while CLP resulted in 12.5% mortality. One-way ANOVAs on food consumption relative to body weight during the 24h before surgery did not reveal any differences between animals to be allocated to treatment groups. However, a Mann-Whitney U-test on food consumption relative to body weight during the 24h after the start of surgery showed a significant lower food intake in animals that underwent CLP as compared to sham-operated rats (U: 26.0, $p<0.05$) (Fig. 2A). Mann-Whitney tests on corneal, pinna and righting reflexes showed that CLP significantly reduced the righting reflex 8 (U: 10.0, $p<0.001$) and 24h (U: 4.50, $p<0.001$) later as compared to sham surgery (Fig. 2B) without affecting the pinna and corneal reflexes (Fig. 2C, D).

CLP increased T2-weighted intensities in cortex and striatum

One way ANOVAs on T2-weighted intensity ratios (VOIs of interest relative to that of skull muscle) showed significantly greater maximum and average intensities at the base of the brain ($F_{1,17}$: 8.98, $p<0.01$; Fig. 3A; $F_{1,17}$: 16.4, $p<0.001$ (data not shown), respectively) in CLP animals as compared to sham-operated rats. Similar analyses in the cortex also indicated a greater maximum ($F_{1,18}$: 5.41, $p<0.05$; Fig. 3B) in CLP rats compared to sham-surgery controls, but no effect on average intensity. In the striatum, one way ANOVAs showed greater maximum and average intensities ($F_{1,18}$: 5.39, $p<0.05$; Fig. 3C; $F_{1,18}$: 6.99, $p<0.05$ (data not shown), respectively) 24h after CLP compared to sham-surgery. Finally, one way ANOVAs only revealed a trend for an increased maximum in the corpus callosum ($F_{1,18}$: 4.08, $p=0.059$; Fig. 3D) of CLP animals as compared to sham-operated rats with no differences in average intensities.

CLP decreased perfusion towards the cerebral cortex

One-way ANOVAs or Mann-Whitney tests on absolute perfusion values in the ROIs covering the cortex (Sham: 105.75 ± 7.29ml/100g/min; CLP: 97.97 ± 5.46ml/100g/min), striatum (Sham 102.56 ± 10.71ml/100g/min; CLP: 96.7 ± 7.24ml/100g/min), corpus callosum (Sham: 112.85 ± 9.07ml/100g/min; CLP 101.28 ± 7.77ml/100g/min) and external capsule (Sham: 94.21 ± 8.48ml/100g/min; CLP 87.07 ± 4.88ml/100g/min) did not reveal significant differences between CLP- and sham surgery groups 24 h after surgery.

To assess the distribution of blood between brain structures, perfusion values measured in brain areas were also analyzed relative to that of the hemisphere (or to that of the global brain parenchyma in the case of the ROI centered on the corpus callosum that is situated between the two hemispheres). One-way ANOVAs on these data indicated significant lower distribution of blood to the cortex ($F_{1,18}$: 5.04, $p<0.05$; Fig. 4A), but no changes in perfusion distribution to the striatum (Fig. 4B), corpus callosum (Fig. 4C) or external capsule region (Fig. 4D) in animals that had undergone CLP surgery as compared to sham surgery.

CLP increased axial water diffusion in the corpus callosum

DWI data were generally of good comparable quality in 20 out of 21 animals. One animal was excluded because its head was tilted in a way that hindered processing for DTI.

Mann-Whitney tests on water diffusion parameters in the ROI covering the cortex at the anatomical level where the white matter of the anterior commissure crosses the third ventricle (corresponding to bregma -0.51mm (Swanson, 1998)) or at the level where the third ventricle is divided in a ventral and dorsal part by the grey matter of the paraventricular thalamus, (corresponding to bregma -1.08mm (Swanson, 1998)) did not indicate any significant differences between rats that underwent CLP and those that were subject to sham surgery.

Similar analyses on water diffusion parameters in the striatum ROI indicated a significant decrease in RD at bregma -1.08mm ($F_{1,18}$: 4.82, $p<0.05$). Using a non-hypothesis-driven and non-ROI-based TBSS approach, a significant higher FA was found in the ventral caudate putamen and globus pallidus of images centered at bregmas -0.51 and -0.83mm of CLP rats as compared to sham-operated animals after 5000 random permutations (Supplementary fig. 1).

One-way ANOVAs or Mann-Whitney tests on water diffusion parameters measured in the corpus callosum ROI at bregma -0.51mm indicated a significant increase in λ1 (U: 19.0, $p<0.05$; Fig. 5A) and a significant decrease in Cp (U: 18.0, $p<0.05$) in rats that underwent CLP surgery as compared to sham-operated rats.

Finally, one-way ANOVAs or Mann-Whitney tests on water diffusion parameters in the ROI placed on the external capsule at bregma -1.08mm revealed a significant increase in FA in the left external capsule ($F_{1,18}$: 5.33, $p<0.05$; Fig. 5B) after CLP as compared to sham surgery.

CLP did not induce widespread BBB breakdown

In all animals, IgG was found in brain regions lacking a functional BBB including the choroid plexus, meninges and circumventricular organs from which it spread to surrounding regions (Fig. 6A, B). One-way ANOVA or Mann-Whitney tests on the occurrence of perivascular plume-like diffusion clouds of IgG staining in the white matter revealed a significantly increased frequency in the fimbria (U: 30.0, $p<0.05$; not shown), but not in the corpus callosum (Fig. 6C, D) or elsewhere in the white matter (Fig. 6E, F), of rats that underwent sham surgery as compared to CLP animals. Similar analyses on grey matter did not indicate any differences with regard to the light to moderate perivascular IgG diffusion that was occasionally observed in the cortex, striatum and hippocampus of both sham-operated and CLP animals (Fig. 6G-J).

CLP decreased cortical COX-2-immunoreactivity

No or very weak COX-2 immunoreactivity was found associated with blood vessels in the preoptic area (Fig. 7A), caudate putamen (Fig. 7C), external capsule (Fig. 7E), hippocampus (Fig. 7G) or cortex (Fig. 7I) of animals subjected to sham-surgery. However, distinct perivascular disc-like COX-2-immunoreactive cells were frequently observed in these structures, with the exception of the hippocampus, in rats that underwent CLP (Fig. 7B, D, F, H and J).

Constitutive COX-2 expression was detected in neurons of the hippocampus and to a lesser extent, in neurons of the cortex (Fig. 7 G-J). Interestingly, and in spite of perivascular induction of COX-2 in the cortex, one-way ANOVAs on cortical COX-2-immunoreactivity showed a significant decrease in the number of cells ($F_{1,11}$: 22.2, $p<0.001$), the total ($F_{1,11}$: 8.37, $p<0.05$) and relative ($F_{1,11}$: 8.90, $p<0.05$) surface labeled after CLP in comparison to sham-surgery (Fig. 7K, L). Interestingly, significant positive correlations were found between the total and relative surface occupied by COX-2 immunoreactivity and perfusion distribution to the cortex (both $r=0.75$, $p<0.005$).

CLP altered microglial density and morphology in grey and white matter

One-way ANOVAs on Iba-1 staining in the cortex revealed a significant increase in the number ($F_{1,15}$: 8.68, $p<0.05$) and relative surface ($F_{1,15}$: 7.46, $p<0.05$) of positive elements in CLP rats compared to sham-operated animals. Similar analyses on Iba-1-immunoreactivity in the striatum also indicated a significant increase in number ($F_{1,16}$: 6.15, $p<0.05$) and relative surface labeled ($F_{1,16}$: 6.29, $p<0.05$) after CLP rats as compared to sham surgery. In addition, one-way ANOVAs on Iba-1 staining in the ventral part of the striatum at bregma levels -0.51 to -0.83mm, that was indicated by tract-based spatial statistics of water diffusion data,

indicated a significant increase in relative surface ($F_{1,16}$: 5.48, $p<0.05$) of positive elements in CLP rats as compared to sham-operated animals. Finally, a significant negative correlation was found between the number of Iba-1-immunoreactive elements and MD in the striatum at bregma -1.08mm ($r=-0.50$, $p<0.05$).

In contrast, one-way ANOVAs on Iba-1 staining in the corpus callosum (Fig. 8A, B) did not reveal a significant difference in relative surface of positive elements in CLP rats as compared to sham-operated animals. However, one-way ANOVAs or Mann-Whitney tests on other measures obtained by fractal analysis showed a significant increase in area (U: 21.0, $p<0.05$), perimeter (U=21.0, $p<0.05$), height ($F_{1,18}$: 14.9, $p<0.01$; Fig. 8C) and width ($F_{1,18}$: 6.93, $p<0.05$; Fig. 8D) of Iba-1-positive elements in CLP rats compared to sham-operated animals. One-way ANOVAs or Mann-Whitney tests on parameters generated by the method of Hovens et al. (2014) indicated a significant decrease in Iba-1-positive cell size (U:18.0, $p<0.05$) and cell processes (U: 18.0, $p<0.05$) and a significantly increased cell body size (U: 0.0, $p<0.001$) as well as a significantly increased microglial activation measure (cell body size/cell size; $F_{1,17}$: 6.94, $p<0.05$) in CLP animals compared to sham-operated rats. Linear regression analyses did not indicate any significant correlations between measures of Iba-1-immunoreactivity and increased axial diffusion in the corpus callosum.

CLP altered corpus callosum astroglia morphology, but not density

One-way ANOVAs on GFAP staining in the cortex revealed a significant increase in the number ($F_{1,19}$: 4.91, $p<0.05$) and relative surface ($F_{1,19}$: 4.55, $p<0.05$) of positive elements in CLP rats compared to sham-operated animals. Similar analyses on GFAP-immunoreactivity in the striatum also indicated a significant increase in number ($F_{1,19}$: 6.14, $p<0.05$) and relative surface labeled ($F_{1,19}$: 5.82, $p<0.05$) in after CLP as compared to sham surgery. Finally, a one-way ANOVA on GFAP staining in the ventral region of the striatum at bregma

levels -0.51 and -0.83mm, indicated by tract-based spatial statistics to show changes in water diffusion, showed a trend for an increase in number ($F_{1,13}$: 4.57, p=0.052) of GFAP-positive elements.

One-way ANOVAs or Mann-Whitney tests on GFAP staining in the corpus callosum (Fig. 9A, B) did not reveal any differences in number or relative surface of positive elements between CLP rats and sham-operated animals. One-way ANOVAs on fractal parameters of GFAP-1-positive cells in the corpus callosum also did not indicate significant differences in height (Fig. 9C), width, perimeter, surface and circularity.

One-way ANOVAs on GFAP-positive fragments (<300 pixels) in the corpus callosum using a fixed threshold did however indicate a significantly lower number of counts ($F_{1,17}$: 8.45, $p<0.05$) and relative surface ($F_{1,17}$: 18.49, $p<0.001$; Fig. 9D) in the CLP group as compared to sham surgery. Interestingly, significant negative correlations were found between the number of and the relative surface occupied by GFAP-positive fragments and axial water diffusion ($r=-0.63$, $p<0.01$ and $r=-0.70$, $p<0.005$, respectively) in the corpus callosum.

CLP decreased cortical AQP4 expression

One way ANOVA showed that cortical AQP4-immunoreactivity (Fig. 10A, B) between bregma -0.46 and -1.08 mm, which corresponded to the position of the T2-weighted image analyzed above, was significantly lower 24h after CLP-induced sepsis than after sham surgery in terms of both counts ($F_{1,14}$:9.74, $p<0.01$; Fig. 10C) and relative surface ($F_{1,14}$:8.66, $p<0.05$; Fig. 10D). Similar analyses on AQP4-positive staining in the corpus callosum and striatum did not indicate differences between groups. In addition, no significant correlations were found between AQP4-immunoreactivity and T2-weighted images in any of these brain structures.

Discussion

The main findings of the present work were that CLP induced sepsis-associated CNS dysfunction resulted in higher T2-weighted contrast intensities in the cortex, striatum and at the base of the brain, decreased blood perfusion distribution to the cortex and increased axial water diffusion in the corpus callosum and fractional anisotropy in the ventral striatum compared to sham surgery. In these animals, CLP induced perivascular COX-2 expression, decreased cortical COX-2 and AQP4 expression and altered white matter glial cell morphology. Interestingly, positive correlations were established between COX-2 immunoreactivity and perfusion distribution to the cortex, while negative correlations were found between GFAP-positive fragments and axial water diffusion in the corpus callosum.

Decreased food intake is a classic non-specific symptom of systemic inflammation in response to bacterial infection (Hart, 1988; Konsman and Dantzer, 2001) and was observed following CLP. In addition, the loss of the righting reflex in animals that underwent CLP is in agreement with previous studies (Kadoi and Goto, 2004; Kafa et al., 2010a; Kafa et al., 2010b) and indicated deteriorated neurological status and SAE**.**

Using the perivascular diffusion of IgG as a marker of BBB breakdown, no indication of increased BBB permeability was found in the parenchyma of the grey and white matter, except for the fimbria, after CLP in the present work. This was neither due to technical failure nor lack of sensitivity as perivascular IgG was readily observed in brain circumventricular organs and meninges, where the endothelial BBB is absent. Moreover, we recently showed increased perivascular IgG diffusion in the white matter after ip LPS administration using the same staining protocol (Dhaya et al., 2018). It is important to keep in mind however that the severity of CLP-induced sepsis depends on the size of the needle used to puncture as well as the number of punctures (Rittirsch et al., 2009) and that the needle size used here was smaller than previous work reporting BBB breakdown 24h after CLP in rodents (Avtan et al., 2011;

Comim et al., 2011; Imamura et al., 2011; Jeppson et al., 1981; Vachharajani et al., 2012; Yokoo et al., 2012). Given that SAE has been proposed to be related to BBB breakdown (Chaudhry and Duggal, 2014; Papadopoulos et al., 2000; Tsuruta and Oda, 2016), our experimental model is interesting in that it induces signs of neurological impairment in the absence of widespread BBB breakdown for molecules of high molecular weight.

Behavioral impairment was associated with signs of fluid accumulation at the base of the brain as indicated by increased T2-weighted contrast, which is in accordance with results of T2-weighted imaging in a murine CLP model (Bozza et al., 2010). In addition, increased T2-weighted contrast intensities were also found in the cortex and striatum in the present work. As diffusion imaging did not indicate altered ADC in the cortex and striatum the increase in T2 intensities were considered as indicating vasogenic rather than cytotoxic edema (Loubinoux et al., 1997). Interestingly, lower perivascular expression of the water channel AQP4 was observed in the cortex of CLP animals as compared to those subject to sham surgery. Reduced water clearance may therefore, in part, explain the increased T2-weighted contrast intensity found in the cortex after CLP.

Since in addition to edema, SAE has been proposed to be related to reduced CBF and oxygen extraction (Papadopoulos et al., 2000), the perfusion of major brain was assessed with ASL. The accuracy of ASL-FAIR to quantify brain perfusion in the rat at low, normal, and moderately increased flows has been validated by a direct comparison with the cerebral distribution of intravenously-injected radioactive microspheres (Bos et al., 2012). Brain perfusion values in sham-operated animals were in accordance with those observed in some previous studies (Detre et al., 1992; Williams et al., 1992), but higher than those described by others (Danker and Duong, 2007; Shen et al., 2016), yet lower than measured in still other published work (Carr et al., 2007; Moffat et al., 2005; Williams et al., 1992). These discrepancies may be due to differences in anesthesia, ASL sequences used and the way the

brain was defined (in our case both cerebral hemispheres without the ventricular system and the large vessels at the base of the brain). This being said, ASL-based perfusion data are known to vary even between studies of the same group (Danker and Duong, 2007; Shen et al., 2016; Sicard et al., 2003) and the aim of the present work was not to obtain absolute quantitative, but to compare between CLP and sham-surgery.

Like in our previous work with LPS (Dhaya et al., 2018), perfusion of the global brain, striatum and cortex was not found to be altered by CLP-induced sepsis. In addition, to absolute perfusion values, the distribution of blood between brain structures is an important value as this distribution can vary as a function of local cerebral metabolism. In this respect it is interesting to note that the distribution of blood to the cortex relative to that of the ipsilateral hemisphere was lower 24h after CLP as compared to sham-surgery. This relative hypoperfusion of the cortex may be related to a loss of cerebral autoregulation or uncoupling between CBF and cerebral metabolism (Feng et al., 2010; Rosengarten et al., 2007). The reported local decrease of glucose utilization in cortical areas (Soejima et al., 1990) and altered cortical electric activity (Kafa et al., 2010a) during sepsis support the possibility of altered cortical metabolism. Cortical COX-2 plays an important role in neurovascular coupling between neuronal activity and CBF (Niwa et al., 2000; Stefanovic et al., 2006). Interestingly although increased perivascular *de novo* induction of perivascular COX-2 was observed after CLP, overall cortical COX-2-immunoreactivity was decreased as compared to sham-surgery. Moreover, significant positive correlations were found between the total and relative surface occupied by COX-2 immunoreactivity and perfusion distribution to the cortex indicating that these imaging and histological measures varied to the same extent. Thus, decreased neuronal COX-2 may explain the observed decrease in blood distribution towards the cerebral cortex during sepsis.

In accordance with and expanding our previous work on LPS, increased axial water diffusion

was observed in the body of corpus callosum after CLP. The body of the corpus callosum is characterized by large axonal diameter distribution and a higher diffusivity suggesting that the space between axons may be larger than that in the genu and splenium where axonal diameter is lower (Barazany et al., 2009). The observed decrease in the coefficient of planar anisotropy in the corpus callosum may also be explained by increased axial water diffusion as $\lambda 1$ is part of the divider term that allows to calculate planar anisotropy ($Cp = 2(\lambda 2 - \lambda 3)/(\lambda 1 + \lambda 2 + \lambda 3)$). Of note, septic patients that had suffered from SAE show an inverse correlation between delirium duration and FA in the body of the corpus callosum three months later, but not at hospital discharge (Morandi et al., 2012). The shape-oriented anisotropy measure Cp has been shown to be more useful than FA to differentiate between white matter fibers and abscesses, between white matter and tumors and between invasive and well-demarcated tumors in the brain (Kim et al., 2008; Kumar et al., 2008; Lope-Piedrafita et al., 2008). Collectively, previously-published findings together with the present observations suggest that during inflammation axial diffusion increases while planar anisotropy decreases in the white matter of the corpus callosum first to later give rise to decreased fractional anisotropy. However, lower FA in the splenium and genu, but not in the body, of the corpus callosum at hospital discharge is associated with worse verbal fluency and attention scores months later (Morandi et al., 2012). Interestingly, patients with PTSD, a condition that also often occurs months after sepsis (Boer et al., 2008; Rosendahl et al., 2013; Schelling et al., 2001; Wintermann et al., 2015), do show decreased FA in the body of the corpus callosum when compared with healthy non-trauma-exposed controls as well as a negative correlation between PTSD clinical scores and the corpus callosum body FA (O'Doherty et al., 2018). Thus, our present findings of reduced planar anisotropy in the corpus callosum body 24h after sepsis induction may be relevant for the subsequent of development stress disorder but not for that of cognitive impairment.

Recently, disruption of the tubulin network inside white matter axons has been shown in rats made septic by intraperitoneal injection of fecal slurry (Ehler et al., 2017). If the same phenomenon occurred after CLP, this could alter axial diffusion in the corpus callosum. Interestingly, peripheral administration of the microtubule assembly inhibitor methylmercury increases axial diffusion in rat optic nerves (Kinoshita et al., 1999) and suggests that the increase in axial diffusion as observed in the corpus callosum of septic animals could be related to changes in the intraneuronal tubulin network. Alternatively, retraction of the processes of microglia or astrocytes that occupy the space between white mater fibers may explain increased horizontal water diffusion in the corpus callosum after CLP. Indeed, in the corpus callosum, microglia and astrocytes have several long cytoplasmic processes that run mostly parallel, but also perpendicularly to the longitudinal axis of myelinated axons (Lawson et al., 1990; Mori and Leblond, 1969a, b). In the present work, an increase in Iba-1 positive cell body size, a decrease in cell processes stained for Iba-1and an increase in cell body to cell size ratio were observed in the corpus callosum of CLP animals as compared to that of rats that underwent sham-surgery. This increased cell body to cell size ratio has been proposed as a measure of microglial activation (Hovens et al., 2014). In addition, CLP decreased in the number of GFAP-positive fragments in the corpus callosum. The decrease in Iba-1 positive cell processes and GFAP-immunoreactive fragments may represent retraction of glial processes. This retraction would result in less hindrance for axial water diffusion in the corpus callosum and thus increase it.

When white matter astrocytes are activated, they retract their higher order processes, increase their soma and lose their transverse orientation (Sun et al., 2010). Less GFAP-irmmunorreactive fragments were found in the corpus callosum after CLP than after sham-surgery. Interestingly, significant negative correlations were found between the number of as well as the relative surface occupied by GFAP-positive fragments and axial water diffusion in

the corpus callosum suggesting that changes in this astrocytic marker underlie, at least in part, the observed modifications of dMRI parameters. Although GFAP does not mark astrocytic endfeet (Sun and Jakobs, 2012), this finding can be interpreted to suggest astroglial activation and retraction of their processes, which, like for microglia, allows for increased diffusion of water molecules parallel to corpus callosum fibers.

One of the main differences between the present small animal imaging approach and previous clinical imaging studies on sepsis is the use of anesthesia to prevent movement at the level of the brain. While the effects of isoflurane anesthesia on rodent regional cerebral blood flow is relatively well-known (Sicard et al., 2003), to the best of our knowledge no comparison of white matter diffusion MRI parameters between isoflurane anesthetized and awake rodents has been done to date. Future work will need to address this matter and determine to what extent the present findings are translationally relevant. If the effects of anesthesia turn out to be negligible, then longitudinal MRI studies of experimental SAE can be envisioned.

In conclusion, our findings confirm the existence of brain dysfunction and increased T2-weighted contrast at the base of the brain 24 h after CLP in rodents. In addition, they expand previous findings in showing increased T2-weighted contrast in the striatum and cortex, decreased perfusion distribution to the cortex and increased axial water diffusion in the corpus callosum. Importantly, these imaging findings were accompanied by lower numbers of Iba-1- and GFAP-immunoreactive fragments in the corpus callosum, decreased neuronal COX-2 and AQP4 expression in the cortex, but not by widespread perivascular IgG diffusion indicating breakdown of the BBB. Collectively, these findings indicate that early SAE is related to changes in cerebral blood flow and white matter microstructure, but not to BBB breakdown.

Acknowledgements

This work was supported by public grants from the French Agence Nationale de la Recherche within the context of the Investments for the Future program referenced ANR-10-LABX-57 named TRAIL (project HR-dMRI).

References

Abdel-Aty, H., Boye, P., Zagrosek, A., Wassmuth, R., Kumar, A., Messroghli, D., Bock, P., Dietz, R., Friedrich, M.G., Schulz-Menger, J., 2005. Diagnostic performance of cardiovascular magnetic resonance in patients with suspected acute myocarditis: comparison of different approaches. J Am Coll Cardiol 45, 1815-1822.

Alexander, A.L., Hasan, K., Kindlmann, G., Parker, D.L., Tsuruda, J.S., 2000. A geometric analysis of diffusion tensor measurements of the human brain. Magn Reson Med 44, 283-291.

Avtan, S.M., Kaya, M., Orhan, N., Arslan, A., Arican, N., Toklu, A.S., Gurses, C., Elmas, I., Kucuk, M., Ahishali, B., 2011. The effects of hyperbaric oxygen therapy on blood-brain barrier permeability in septic rats. Brain Res 1412, 63-72.

Barazany, D., Basser, P.J., Assaf, Y., 2009. In vivo measurement of axon diameter distribution in the corpus callosum of rat brain. Brain 132, 1210-1220.

Bartynski, W.S., Boardman, J.F., Zeigler, Z.R., Shadduck, R.K., Lister, J., 2006. Posterior reversible encephalopathy syndrome in infection, sepsis, and shock. AJNR Am J Neuroradiol 27, 2179-2190.

Boer, K.R., van Ruler, O., van Emmerik, A.A., Sprangers, M.A., de Rooij, S.E., Vroom, M.B., de Borgie, C.A., Boermeester, M.A., Reitsma, J.B., Dutch Peritonitis Study, G., 2008. Factors associated with posttraumatic stress symptoms in a prospective cohort of patients after abdominal sepsis: a nomogram. Intensive Care Med 34, 664-674.

Bos, A., Bergmann, R., Strobel, K., Hofheinz, F., Steinbach, J., den Hoff, J., 2012. Cerebral blood flow quantification in the rat: a direct comparison of arterial spin labeling MRI with radioactive microsphere PET. EJNMMI Res 2, 47.

Bowton, D.L., Bertels, N.H., Prough, D.S., Stump, D.A., 1989. Cerebral blood flow is reduced in patients with sepsis syndrome. Crit Care Med 17, 399-403.

Bozza, F.A., Garteiser, P., Oliveira, M.F., Doblas, S., Cranford, R., Saunders, D., Jones, I., Towner, R.A., Castro-Faria-Neto, H.C., 2010. Sepsis-associated encephalopathy: a magnetic resonance imaging and spectroscopy study. J Cereb Blood Flow Metab 30, 440-448.

Bryan, W.J., Emerson, T.E., Jr., 1977. Blood flow in seven regions of the brain during endotoxin shock in the dog. Proc Soc Exp Biol Med 156, 205-208.

Carr, J.P., Buckley, D.L., Tessier, J., Parker, G.J., 2007. What levels of precision are achievable for quantification of perfusion and capillary permeability surface area product using ASL? Magn Reson Med 58, 281-289.

Chaudhry, N., Duggal, A.K., 2014. Sepsis Associated Encephalopathy. Adv Med 2014, 762320.

Christenson, J.T., Kuikka, J.T., Owunwanne, A., Al-Sarraf, A.A., 1986. Cerebral circulation during endotoxic shock with special emphasis on the regional cerebral blood flow in vivo. Nucl Med Commun 7, 531-540.

Comim, C.M., Vilela, M.C., Constantino, L.S., Petronilho, F., Vuolo, F., Lacerda-Queiroz, N., Rodrigues, D.H., da Rocha, J.L., Teixeira, A.L., Quevedo, J., Dal-Pizzol, F., 2011. Traffic of leukocytes and cytokine up-regulation in the central nervous system in sepsis. Intensive Care Med 37, 711-718.

Danker, J.F., Duong, T.Q., 2007. Quantitative regional cerebral blood flow MRI of animal model of attention-deficit/hyperactivity disorder. Brain Res 1150, 217-224.

Detre, J.A., Leigh, J.S., Williams, D.S., Koretsky, A.P., 1992. Perfusion imaging. Magn Reson Med 23, 37-45.

Dhaya, I., Griton, M., Raffard, G., Amri, M., Hiba, B., Konsman, J.P., 2018. Bacterial lipopolysaccharide-induced systemic inflammation alters perfusion of white matter-rich regions without altering flow in brain-irrigating arteries: Relationship to blood-brain

barrier breakdown? J Neuroimmunol 314, 67-80.

Dobre, M.C., Ugurbil, K., Marjanska, M., 2007. Determination of blood longitudinal relaxation time (T1) at high magnetic field strengths. Magn Reson Imaging 25, 733-735.

Ebersoldt, M., Sharshar, T., Annane, D., 2007. Sepsis-associated delirium. Intensive Care Med 33, 941-950.

Ehler, J., Barrett, L.K., Taylor, V., Groves, M., Scaravilli, F., Wittstock, M., Kolbaske, S., Grossmann, A., Henschel, J., Gloger, M., Sharshar, T., Chretien, F., Gray, F., Noldge-Schomburg, G., Singer, M., Sauer, M., Petzold, A., 2017. Translational evidence for two distinct patterns of neuroaxonal injury in sepsis: a longitudinal, prospective translational study. Crit Care 21, 262.

Ekstrom-Jodal, B., Haggendal, J., Larsson, L.E., Westerlind, A., 1982. Cerebral hemodynamics, oxygen uptake and cerebral arteriovenous differences of catecholamines following E. coli endotoxin in dogs. Acta Anaesthesiol Scand 26, 446-452.

Esparza-Coss, E., Wosik, J., Narayana, P.A., 2010. Perfusion in rat brain at 7 T with arterial spin labeling using FAIR-TrueFISP and QUIPSS. Magn Reson Imaging 28, 607-612.

Feng, S.Y., Samarasinghe, T., Phillips, D.J., Alexiou, T., Hollis, J.H., Yu, V.Y., Walker, A.M., 2010. Acute and chronic effects of endotoxin on cerebral circulation in lambs. Am J Physiol Regul Integr Comp Physiol 298, R760-766.

Gofton, T.E., Young, G.B., 2012. Sepsis-associated encephalopathy. Nat Rev Neurol 8, 557-566.

Hart, B.L., 1988. Biological basis of the behavior of sick animals. Neurosci Biobehav Rev 12, 123-137.

Hinkelbein, J., Schroeck, H., Peterka, A., Schubert, C., Kuschinsky, W., Kalenka, A., 2007. Local cerebral blood flow is preserved in sepsis. Curr Neurovasc Res 4, 39-47.

Hoogland, I.C., Houbolt, C., van Westerloo, D.J., van Gool, W.A., van de Beek, D., 2015.

Systemic inflammation and microglial activation: systematic review of animal experiments. J Neuroinflammation 12, 114.

Hovens, I.B., Nyakas, C., Schoemaker, R.G., 2014. A novel method for evaluating microglial activation using ionized calcium-binding adaptor protein-1 staining: cell body to cell size ratio. Neuroimmunol Neuroinflammation 1, 82-88.

Imamura, Y., Wang, H., Matsumoto, N., Muroya, T., Shimazaki, J., Ogura, H., Shimazu, T., 2011. Interleukin-1beta causes long-term potentiation deficiency in a mouse model of septic encephalopathy. Neuroscience 187, 63-69.

Jeppson, B., Freund, H.R., Z., G., James, J.H., von Meyenfeldt, M.F., J.E., F., 1981. Blood-brain barrier derangement in sepsis: cause of septic encephalopathy? Am J Surg 141, 136-142.

Jones, C., Griffiths, R.D., 2013. Mental and physical disability after sepsis. Minerva Anestesiol 79, 1306-1312.

Kadoi, Y., Goto, F., 2004. Selective inducible nitric oxide inhibition can restore hemodynamics, but does not improve neurological dysfunction in experimentally-induced septic shock in rats. Anesth Analg 99, 212-220.

Kafa, I.M., Bakirci, S., Uysal, M., Kurt, M.A., 2010a. Alterations in the brain electrical activity in a rat model of sepsis-associated encephalopathy. Brain Res 1354, 217-226.

Kafa, I.M., Uysal, M., Bakirci, S., Ayberk Kurt, M., 2010b. Sepsis induces apoptotic cell death in different regions of the brain in a rat model of sepsis. Acta Neurobiol Exp (Wars) 70, 246-260.

Kim, S., Pickup, S., Hsu, O., Poptani, H., 2008. Diffusion tensor MRI in rat models of invasive and well-demarcated brain tumors. NMR Biomed 21, 208-216.

Kinoshita, Y., Ohnishi, A., Kohshi, K., Yokota, A., 1999. Apparent diffusion coefficient on rat brain and nerves intoxicated with methylmercury. Environ Res 80, 348-354.

Kober, F., Iltis, I., Izquierdo, M., Desrois, M., Ibarrola, D., Cozzone, P.J., Bernard, M., 2004. High-resolution myocardial perfusion mapping in small animals in vivo by spin-labeling gradient-echo imaging. Magn Reson Med 51, 62-67.

Konsman, J.P., Blomqvist, A., 2005. Forebrain patterns of c-Fos and FosB induction during cancer-associated anorexia-cachexia in rat. Eur J Neurosci 21, 2752-2766.

Konsman, J.P., Dantzer, R., 2001. How the immune and nervous systems interact during disease-associated anorexia. Nutrition 17, 664-668.

Konsman, J.P., Veeneman, J., Combe, C., Poole, S., Luheshi, G.N., Dantzer, R., 2008. Central nervous action of interleukin-1 mediates activation of limbic structures and behavioural depression in response to peripheral administration of bacterial lipopolysaccharide. Eur J Neurosci 28, 2499-2510.

Konsman, J.P., Vigues, S., Mackerlova, L., Bristow, A., Blomqvist, A., 2004. Rat brain vascular distribution of interleukin-1 type-1 receptor immunoreactivity: relationship to patterns of inducible cyclooxygenase expression by peripheral inflammatory stimuli. J Comp Neurol 472, 113-129.

Kumar, M., Gupta, R.K., Nath, K., Rathore, R.K., Bayu, G., Trivedi, R., Husain, M., Prasad, K.N., Tripathi, R.P., Narayana, P.A., 2008. Can we differentiate true white matter fibers from pseudofibers inside a brain abscess cavity using geometrical diffusion tensor imaging metrics? NMR Biomed 21, 581-588.

Lamar, C.D., Hurley, R.A., Taber, K.H., 2011. Sepsis-associated encephalopathy: review of the neuropsychiatric manifestations and cognitive outcome. J Neuropsychiatry Clin Neurosci 23, 237-241.

Lawson, L.J., Perry, V.H., Dri, P., Gordon, S., 1990. Heterogeneity in the distribution and morphology of microglia in the normal adult mouse brain. Neuroscience 39, 151-170.

Lemstra, A.W., Groen in't Woud, J.C., Hoozemans, J.J., van Haastert, E.S., Rozemuller, A.J.,

Eikelenboom, P., van Gool, W.A., 2007. Microglia activation in sepsis: a case-control study. J Neuroinflammation 4, 4.

Lope-Piedrafita, S., Garcia-Martin, M.L., Galons, J.P., Gillies, R.J., Trouard, T.P., 2008. Longitudinal diffusion tensor imaging in a rat brain glioma model. NMR Biomed 21, 799-808.

Loubinoux, I., Volk, A., Borredon, J., Guirimand, S., Tiffon, B., Seylaz, J., Meric, P., 1997. Spreading of vasogenic edema and cytotoxic edema assessed by quantitative diffusion and T2 magnetic resonance imaging. Stroke 28, 419-426; discussion 426-417.

Maekawa, T., Fujii, Y., Sadamitsu, D., Yokota, K., Soejima, Y., Ishikawa, T., Miyauchi, Y., Takeshita, H., 1991. Cerebral circulation and metabolism in patients with septic encephalopathy. Am J Emerg Med 9, 139-143.

Meagher, D.J., Morandi, A., Inouye, S.K., Ely, W., Adamis, D., Maclullich, A.J., Rudolph, J.L., Neufeld, K., Leonard, M., Bellelli, G., Davis, D., Teodorczuk, A., Kreisel, S., Thomas, C., Hasemann, W., Timmons, S., O'Regan, N., Grover, S., Jabbar, F., Cullen, W., Dunne, C., Kamholz, B., Van Munster, B.C., De Rooij, S.E., De Jonghe, J., Trzepacz, P.T., 2014. Concordance between DSM-IV and DSM-5 criteria for delirium diagnosis in a pooled database of 768 prospectively evaluated patients using the delirium rating scale-revised-98. BMC Med 12, 164.

Moffat, B.A., Chenevert, T.L., Hall, D.E., Rehemtulla, A., Ross, B.D., 2005. Continuous arterial spin labeling using a train of adiabatic inversion pulses. J Magn Reson Imaging 21, 290-296.

Moller, K., Strauss, G.I., Qvist, J., Fonsmark, L., Knudsen, G.M., Larsen, F.S., Krabbe, K.S., Skinhoj, P., Pedersen, B.K., 2002. Cerebral blood flow and oxidative metabolism during human endotoxemia. J Cereb Blood Flow Metab 22, 1262-1270.

Morandi, A., Rogers, B.P., Gunther, M.L., Merkle, K., Pandharipande, P., Girard, T.D.,

Jackson, J.C., Thompson, J., Shintani, A.K., Geevarghese, S., Miller, R.R., 3rd, Canonico, A., Cannistraci, C.J., Gore, J.C., Ely, E.W., Hopkins, R.O., Visions Investigation, V.I.S.N.S., 2012. The relationship between delirium duration, white matter integrity, and cognitive impairment in intensive care unit survivors as determined by diffusion tensor imaging: the VISIONS prospective cohort magnetic resonance imaging study*. Crit Care Med 40, 2182-2189.

Mori, S., Leblond, C.P., 1969a. Electron microscopic features and proliferation of astrocytes in the corpus callosum of the rat. J Comp Neurol 137, 197-225.

Mori, S., Leblond, C.P., 1969b. Identification of microglia in light and electron microscopy. J Comp Neurol 135, 57-80.

Niwa, K., Araki, E., Morham, S.G., Ross, M.E., Iadecola, C., 2000. Cyclooxygenase-2 contributes to functional hyperemia in whisker-barrel cortex. J Neurosci 20, 763-770.

O'Doherty, D.C.M., Ryder, W., Paquola, C., Tickell, A., Chan, C., Hermens, D.F., Bennett, M.R., Lagopoulos, J., 2018. White matter integrity alterations in post-traumatic stress disorder. Hum Brain Mapp 39, 1327-1338.

Papadopoulos, M.C., Davies, D.C., Moss, R.F., Tighe, D., Bennett, E.D., 2000. Pathophysiology of septic encephalopathy: a review. Crit Care Med 28, 3019-3024.

Pfister, D., Siegemund, M., Dell-Kuster, S., Smielewski, P., Ruegg, S., Strebel, S.P., Marsch, S.C., Pargger, H., Steiner, L.A., 2008. Cerebral perfusion in sepsis-associated delirium. Crit Care 12, R63.

Piazza, O., Cotena, S., De Robertis, E., Caranci, F., Tufano, R., 2009. Sepsis associated encephalopathy studied by MRI and cerebral spinal fluid S100B measurement. Neurochem Res 34, 1289-1292.

Pierrakos, C., Antoine, A., Velissaris, D., Michaux, I., Bulpa, P., Evrard, P., Ossemann, M., Dive, A., 2013. Transcranial doppler assessment of cerebral perfusion in critically ill

septic patients: a pilot study. Ann Intensive Care 3, 28.

Pierrakos, C., Attou, R., Decorte, L., Kolyviras, A., Malinverni, S., Gottignies, P., Devriendt, J., De Bels, D., 2014. Transcranial Doppler to assess sepsis-associated encephalopathy in critically ill patients. BMC Anesthesiol 14, 45.

Pollard, V., Prough, D.S., Deyo, D.J., Conroy, B., Uchida, T., Daye, A., Traber, L.D., Traber, D.L., 1997. Cerebral blood flow during experimental endotoxemia in volunteers. Crit Care Med 25, 1700-1706.

Rittirsch, D., Huber-Lang, M.S., Flierl, M.A., Ward, P.A., 2009. Immunodesign of experimental sepsis by cecal ligation and puncture. Nat Protoc 4, 31-36.

Rosendahl, J., Brunkhorst, F.M., Jaenichen, D., Strauss, B., 2013. Physical and mental health in patients and spouses after intensive care of severe sepsis: a dyadic perspective on long-term sequelae testing the Actor-Partner Interdependence Model. Crit Care Med 41, 69-75.

Rosengarten, B., Hecht, M., Auch, D., Ghofrani, H.A., Schermuly, R.T., Grimminger, F., Kaps, M., 2007. Microcirculatory dysfunction in the brain precedes changes in evoked potentials in endotoxin-induced sepsis syndrome in rats. Cerebrovasc Dis 23, 140-147.

Rosengarten, B., Hecht, M., Wolff, S., Kaps, M., 2008. Autoregulative function in the brain in an endotoxic rat shock model. Inflamm Res 57, 542-546.

Schelling, G., Briegel, J., Roozendaal, B., Stoll, C., Rothenhausler, H.B., Kapfhammer, H.P., 2001. The effect of stress doses of hydrocortisone during septic shock on posttraumatic stress disorder in survivors. Biol Psychiatry 50, 978-985.

Schramm, P., Klein, K.U., Falkenberg, L., Berres, M., Closhen, D., Werhahn, K.J., David, M., Werner, C., Engelhard, K., 2012. Impaired cerebrovascular autoregulation in patients with severe sepsis and sepsis-associated delirium. Crit Care 16, R181.

Sharshar, T., Carlier, R., Bernard, F., Guidoux, C., Brouland, J.P., Nardi, O., de la

Grandmaison, G.L., Aboab, J., Gray, F., Menon, D., Annane, D., 2007. Brain lesions in septic shock: a magnetic resonance imaging study. Intensive Care Med 33, 798-806.

Shen, Q., Huang, S., Duong, T.Q., 2016. T2*-weighted fMRI time-to-peak of oxygen challenge in ischemic stroke. J Cereb Blood Flow Metab 36, 283-291.

Sicard, K., Shen, Q., Brevard, M.E., Sullivan, R., Ferris, C.F., King, J.A., Duong, T.Q., 2003. Regional cerebral blood flow and BOLD responses in conscious and anesthetized rats under basal and hypercapnic conditions: implications for functional MRI studies. J Cereb Blood Flow Metab 23, 472-481.

Smith, S.M., Jenkinson, M., Johansen-Berg, H., Rueckert, D., Nichols, T.E., Mackay, C.E., Watkins, K.E., Ciccarelli, O., Cader, M.Z., Matthews, P.M., Behrens, T.E., 2006. Tract-based spatial statistics: voxelwise analysis of multi-subject diffusion data. Neuroimage 31, 1487-1505.

Smith, S.M., Nichols, T.E., 2009. Threshold-free cluster enhancement: addressing problems of smoothing, threshold dependence and localisation in cluster inference. Neuroimage 44, 83-98.

Smith, S.M., Padayachee, S., Modaresi, K.B., Smithies, M.N., Bihari, D.J., 1998. Cerebral blood flow is proportional to cardiac index in patients with septic shock. J Crit Care 13, 104-109.

Soejima, Y., Fujii, Y., Ishikawa, T., Takeshita, H., Maekawa, T., 1990. Local cerebral glucose utilization in septic rats. Crit Care Med 18, 423-427.

Stefanovic, B., Bosetti, F., Silva, A.C., 2006. Modulatory role of cyclooxygenase-2 in cerebrovascular coupling. Neuroimage 32, 23-32.

Sun, D., Jakobs, T.C., 2012. Structural remodeling of astrocytes in the injured CNS. Neuroscientist 18, 567-588.

Sun, D., Lye-Barthel, M., Masland, R.H., Jakobs, T.C., 2010. Structural remodeling of

fibrous astrocytes after axonal injury. J Neurosci 30, 14008-14019.

Swanson, L.W., 1998. Brain Maps: Structure of the Rat Brain. Elsevier, Amsterdam.

Tempel, G.E., Cook, J.A., Wise, W.C., Halushka, P.V., Corral, D., 1986. Improvement in organ blood flow by inhibition of thromboxane synthetase during experimental endotoxic shock in the rat. J Cardiovasc Pharmacol 8, 514-519.

Tsuruta, R., Oda, Y., 2016. A clinical perspective of sepsis-associated delirium. J Intensive Care 4, 18.

Vachharajani, V., Cunningham, C., Yoza, B., Carson, J., Jr., Vachharajani, T.J., McCall, C., 2012. Adiponectin-deficiency exaggerates sepsis-induced microvascular dysfunction in the mouse brain. Obesity (Silver Spring) 20, 498-504.

Villega, F., Delpech, J.C., Griton, M., Andre, C., Franconi, J.M., Miraux, S., Konsman, J.P., 2017. Circulating bacterial lipopolysaccharide-induced inflammation reduces flow in brain-irrigating arteries independently from cerebrovascular prostaglandin production. Neuroscience 346, 160-172.

Wichterman, K.A., Baue, A.E., Chaudry, I.H., 1980. Sepsis and septic shock--a review of laboratory models and a proposal. J Surg Res 29, 189-201.

Williams, D.S., Detre, J.A., Leigh, J.S., Koretsky, A.P., 1992. Magnetic resonance imaging of perfusion using spin inversion of arterial water. Proc Natl Acad Sci U S A 89, 212-216.

Wintermann, G.B., Brunkhorst, F.M., Petrowski, K., Strauss, B., Oehmichen, F., Pohl, M., Rosendahl, J., 2015. Stress disorders following prolonged critical illness in survivors of severe sepsis. Crit Care Med 43, 1213-1222.

Wyler, F., Forsyth, R.P., Nies, A.S., Neutze, J.M., Melmon, K.L., 1969. Endotoxin-induced regional circulatory changes in the unanesthetized monkey. Circ Res 24, 777-786.

Wyler, F., Rutishauser, M., Weisser, K., 1972. Endotoxin induced regional circulatory

reactions in the rabbit with and without halothane anesthesia. J Surg Res 13, 13-19.

Yokoo, H., Chiba, S., Tomita, K., Takashina, M., Sagara, H., Yagisita, S., Takano, Y., Hattori, Y., 2012. Neurodegenerative evidence in mice brains with cecal ligation and puncture-induced sepsis: preventive effect of the free radical scavenger edaravone. PLoS One 7, e51539.

Yokota, H., Ogawa, S., Kurokawa, A., Yamamoto, Y., 2003. Regional cerebral blood flow in delirium patients. Psychiatry Clin Neurosci 57, 337-339.

Young, G.B., 2013. Encephalopathy of infection and systemic inflammation. J Clin Neurophysiol 30, 454-461.

Zrzavy, T., Hoftberger, R., Berger, T., Rauschka, H., Butovsky, O., Weiner, H., Lassmann, H., 2019. Pro-inflammatory activation of microglia in the brain of patients with sepsis. Neuropathol Appl Neurobiol 45, 278-290.

Figure and table legends

Figure 1

Placement of different Region Of Interest 1: hemisphere; 2: corpus callosum; 3 external capsule; 4 cortex and 5: striatum. (ROIs; A) used to analyze perfusion-weighted (example in B), T2-weighted (example in C) and diffusion-weighted images (example in D).

Figure 2

Food intake relative to body weight (A) during 24h after CLP or sham surgery. Group size Sham: n=9; CLP: n=11-12. Reflex scores: Pinna (B), corneal (C) and righting (D) reflexes at 24h, 12h, and 1h prior to surgery then 4h, 8h and 24h later. Group size Sham: n=8-9; CLP: n=8-12.

Figure 3

Changes in T2-weighted intensity at the base of the brain (A), in the cortex (B), striatum (C) and the corpus callosum (D). Graphs represent maximum intensities in the VOI relative to that of the muscle 24h after laparotomy or cecal ligation and puncture. *: $p < 0.05$. Group sizes Sham: n=8; CLP: n=11.

Figure 4

Perfusion distribution to rat cortex (A), striatum (B), corpus callosum (C) and external capsule (D).Graphs represent perfusion relative to both hemispheres for all structures except for the corpus callosum that was expressed relative to global brain 24h after surgery. *: $p < 0.05$; Group sizes Sham: n=8; CLP: n=12.

Figure 5

Changes in corpus callosum axial water diffusion at bregma -0.51mm (A) and left external capsule fractional anisotropy the at bregma -1.08mm (B) 24h after laparotomy or cecal ligation and puncture. *: $p < 0.05$. Group sizes Sham: n=7-8; CLP: n=12.

Figure 6

Photomicrographs illustrating the distribution of rat IgG-immunoreactivity in ventral hippocampal commissure (A,B), the corpus callosum (C,D), external capsule (E,F), dorsoslateral striatum (G,H) and hippocampus (I,J), 24 h after laparotomy (A, C, E, G, I) or cecal ligation and puncture (B, D, F, H, J) in rats. cc: corpus callosum; ec: external capsule; vhc: ventral hippocampal comissure; SFO: subfornical organ. Arrow heads > and < indicate perivascular diffuse cloud-like labeling Scale bar = 100μm.

Figure 7

Photomicrographs illustrating the distribution of COX-2-immunoreactivity in the ventromedial preoptic area (A, B), caudate putamen (C, D), external capsule (E, F), hippocampus (G, H) and cortex (I, J) 24h after laparotomy (A, C, E, G, I) or cecal ligation and puncture in rats (B, D, F, H, J). och: optic chiasm; ec: external capsule. Arrow heads > and < indicate labeling. Scale bar = 100 μm. Quantification of cortical COX-2-immunoreactive cells (K) and surface (L) 24h after cecal ligation and puncture or laparotomy. i.r.: immunoreactivity *: $p < 0.05$. Group sizes Sham: n=6; CLP: n=7.

Figure 8

Photomicrographs illustrating Iba1-ir microglia in the corpus callosum after laparotomy (A) or cecal ligation and puncture (B) in rats. Quantitative Fraclac-based analysis of microglial

height (C) and width (D) in the corpus callosum. i.r.: immunoreactivity *: $p < 0.05$. Group sizes Sham: n=9; CLP: n=11. Scale bar = 100µm.

Figure 9

Photomicrographs illustrating GFAP-ir astrocytes in the corpus callosum after laparotomy (A) or cecal ligation and puncture (B) in rats. Quantitative analysis of astrocyte height (Fraclac; C) and the relative surface occupied by GFAP-ir fragments (D) in the corpus callosum. i.r.: immunoreactivity ***: $p < 0.001$. Group sizes Sham: n=9; CLP: n=11. Scale bar = 100µm.

Figure 10

Photomicrographs illustrating AQP4-ir astrocytes end-feet in the cortex after laparotomy (A) or cecal ligation and puncture (B) in rats. Quantitative analysis of counts (C) and the relative surface occupied (D) by AQP4-ir fragments in the cortex. i.r.: immunoreactivity ***: $p < 0.001$. Group sizes and the surface occupied by AQP-4. Sham: n=7; CLP: n=9. Scale bar = 50µm.

Supplementary figure 1

Location of differences in fractional anisotropy indicated by arrows as found in the left striatum using Voxel-based analysis using tract-based spatial statistics (TBSS) with 5000 permutations in the horizontal (A), sagittal (B) and coronal plane (C).

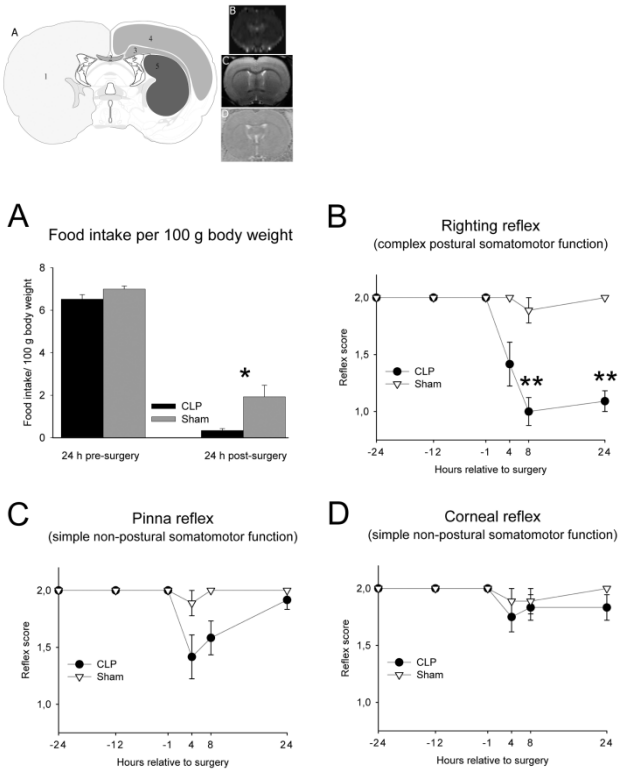

Fig. 2, Griton et al.

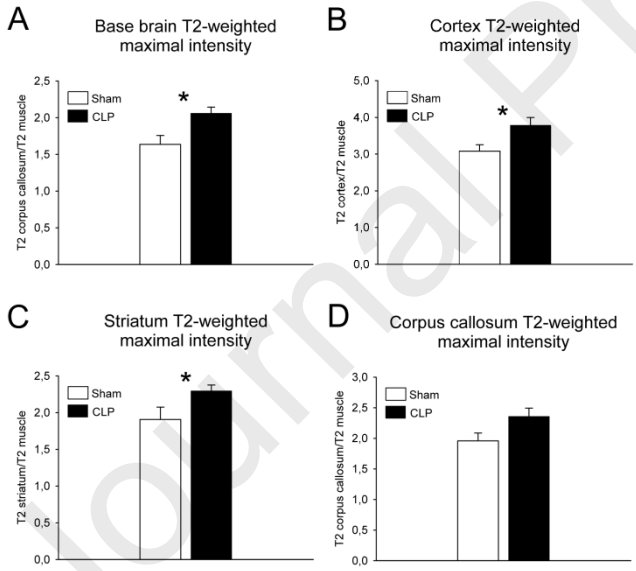

Fig. 3, Griton et al.

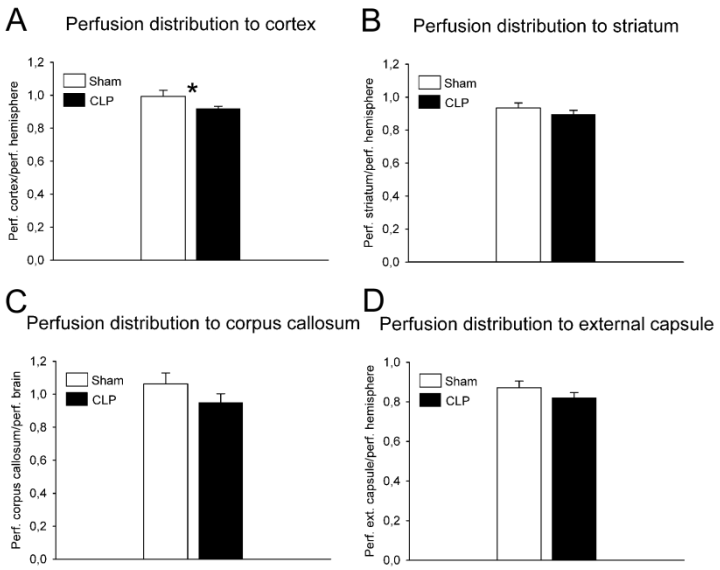

Fig. 4, Griton et al.

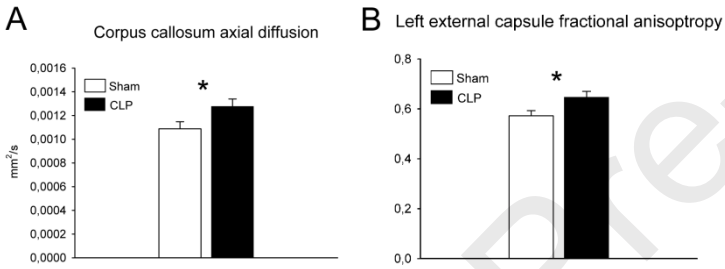

Fig. 5, Griton et al.

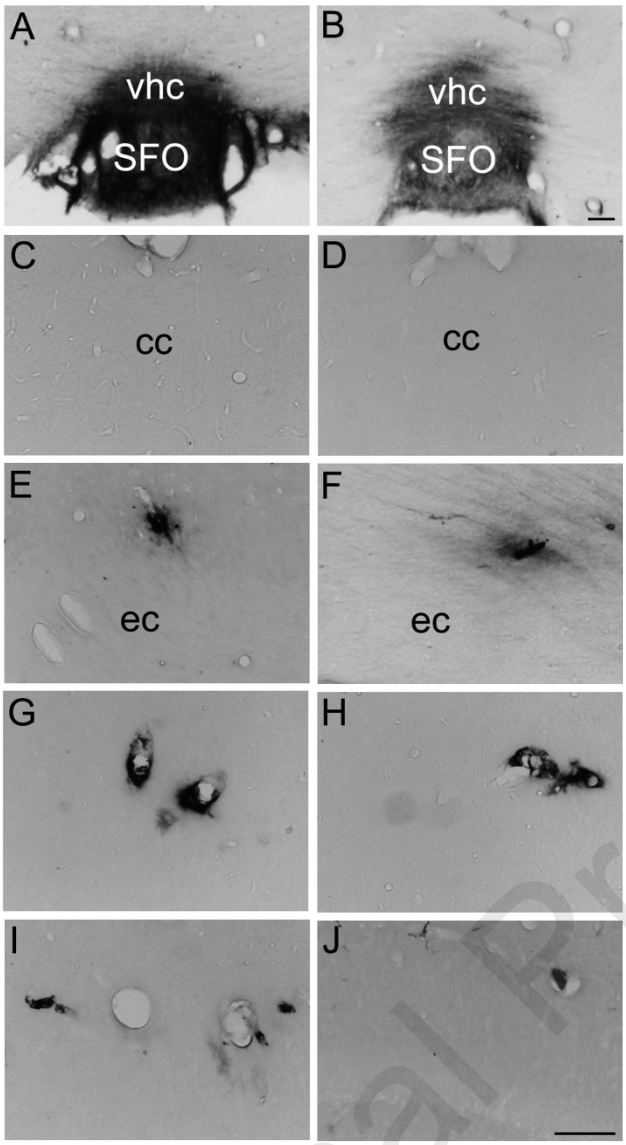

Griton et al., Fig. 6

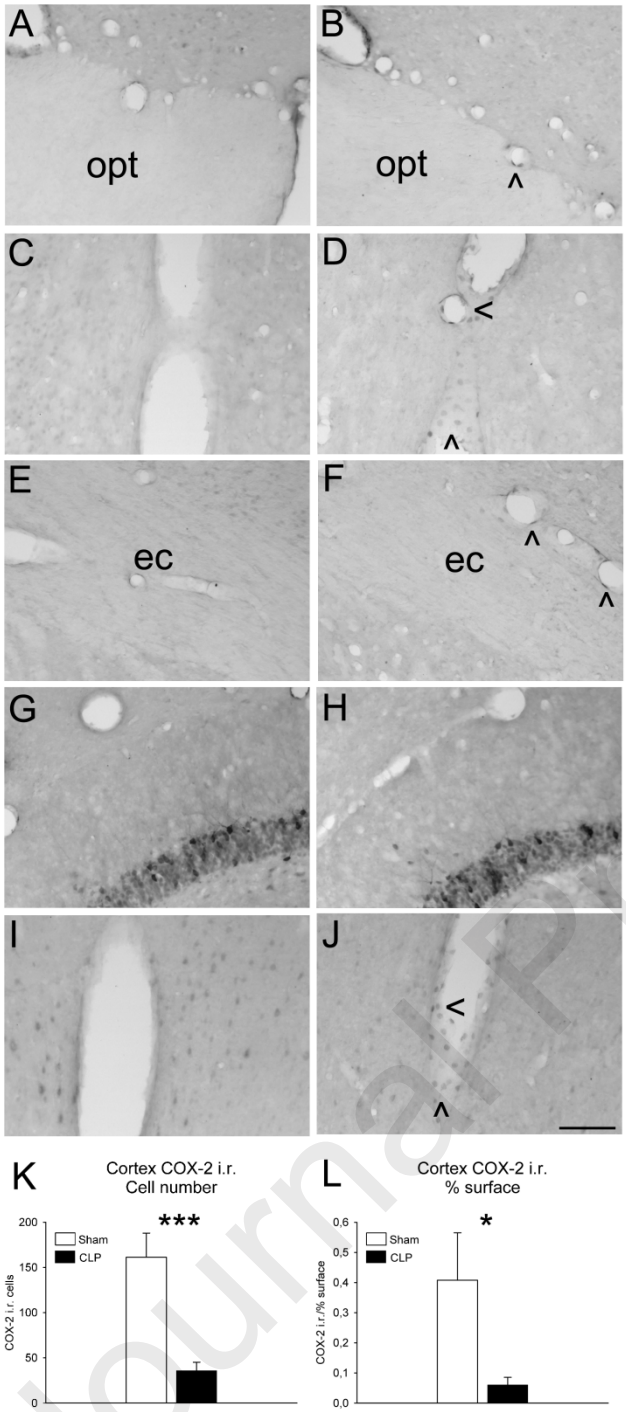

Griton et al., Fig. 7

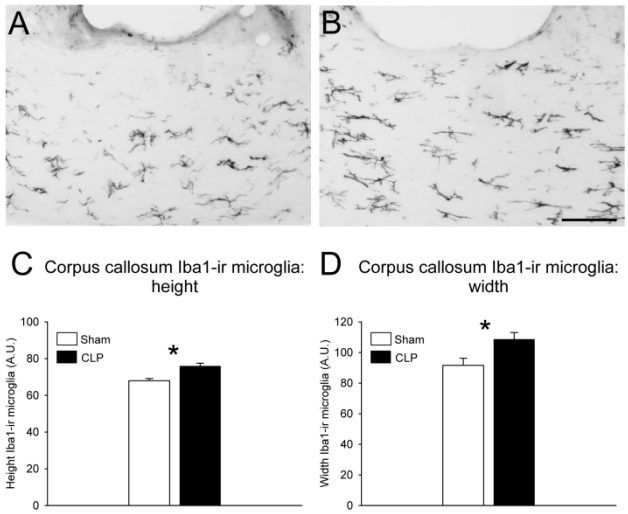

Griton et al., Fig. 8

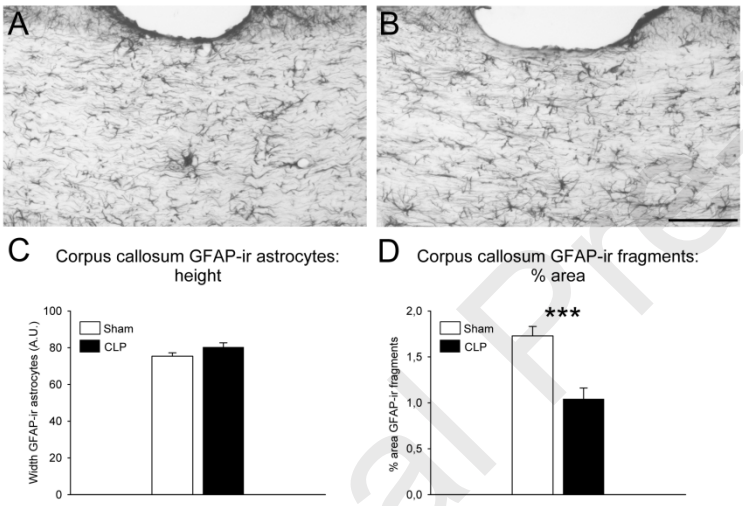

Griton et al., Fig. 9

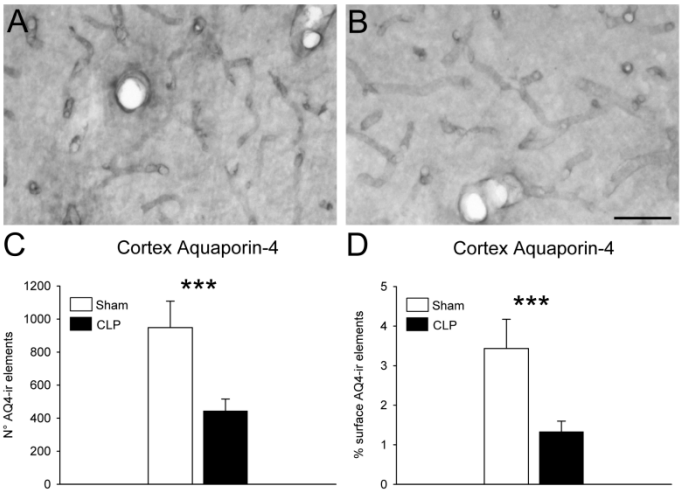

Griton et al., Fig. 10

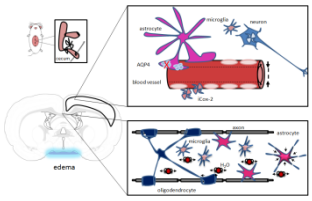

Highlights

Cecal ligation and puncture (CLP) led to encephalopathy

CLP-associated encephalopathy occurred without blood-brain barrier breakdown

CLP decreased blood perfusion distribution to the cortex

CLP decreased cortical cyclooxygenase-2 and aquaporin-4 expression

CLP increased corpus callosum water diffusion and altered glial morphology